POLITECNICO DI TORINO
Repository ISTITUZIONALE

Parameterisation of Radiation Forces for Multiple Degree-of-Freedom Wave Energy Converters Using Moment-Matching

Original
Parameterisation of Radiation Forces for Multiple Degree-of-Freedom Wave Energy Converters Using Moment-Matching / Faedo, Nicolas; Peña-Sanchez, Yerai; Ringwood, John V. - In: INTERNATIONAL JOURNAL OF OFFSHORE AND POLAR ENGINEERING. - ISSN 1053-5381. - 30:4(2020), pp. 395-402. [10.17736/ijope.2020.mk71]

Availability:
This version is available at: 11583/2988053 since: 2024-04-24T08:38:15Z

Publisher:
INT SOC OFFSHORE POLAR ENGINEERS

Published
DOI:10.17736/ijope.2020.mk71

Terms of use:

This article is made available under terms and conditions as specified in the corresponding bibliographic description in the repository

Publisher copyright

(Article begins on next page)

05 February 2025

ResearchGate

See discussions, stats, and author profiles for this publication at: https://www.researchgate.net/publication/346565745

Parameterisation of Radiation Forces for Multiple Degree-of-Freedom Wave Energy Converters Using Moment-Matching

Article *in* International Journal of Offshore and Polar Engineering · December 2020

DOI: 10.17736/ijope.2020.mk71

CITATION
1

READS
118

3 authors:

Nicolás Faedo
Politecnico di Torino
60 PUBLICATIONS **578** CITATIONS
SEE PROFILE

Yerai Peña Sanchez
Universidad del País Vasco / Euskal Herriko Unibertsitatea
28 PUBLICATIONS **258** CITATIONS
SEE PROFILE

John Ringwood
Maynooth University
428 PUBLICATIONS **7,088** CITATIONS
SEE PROFILE

Some of the authors of this publication are also working on these related projects:

Wave energy control systems View project

Application of anti-windup compensation to the control of Wave Energy Converters View project

All content following this page was uploaded by Nicolás Faedo on 02 December 2020.

The user has requested enhancement of the downloaded file.

Parameterisation of Radiation Forces for Multiple Degree-of-Freedom Wave Energy Converters Using Moment-Matching

Nicolás Faedo, Yerai Peña-Sanchez, and John V. Ringwood
Centre for Ocean Energy Research, Maynooth University, Maynooth, Ireland

The motion of a wave energy converter (WEC) can be described in terms of an integro-differential equation, which involves a convolution operator. This convolution term accounts for the effect of radiation forces acting on the device and represents a computational and representational drawback both for simulation and analysis/design of control/estimation strategies. We present herein a moment-based strategy to compute a parametric form of the radiation force subsystem for multiple degree-of-freedom WECs. The strategy allows for the computation of a model that exactly matches the steady-state behaviour of the target system at a set of user-defined frequencies, while retaining the underlying physical properties of radiation forces. The potential and capabilities of the presented method are illustrated considering a CorPower-like device (heaving point absorber) as an application case.

KEY WORDS: Radiation forces, parametric form, model order reduction, frequency-domain identification, moment-matching.

INTRODUCTION

Among the different modelling approaches adopted in the wave energy literature (see (Li and Yu, 2012)), the speed with which numerical simulation may be performed makes the widely known boundary element method (BEM) a common choice to compute hydrodynamic parameters for a given wave energy converter (WEC) (Penalba et al., 2017). However, one of the major drawbacks of the BEM is that the results are computed in the frequency domain and, hence, can only characterise the steady-state motion of the WEC under analysis. Seeking a more comprehensive approach and following the well-known theory developed in (Cummins, 1962), the motion of a WEC can be expressed, in the time domain, using a particular well-known integro-differential equation of the convolution class. The presence of these convolution terms accounts for the effect of radiation forces acting on each of the different degrees of freedom (DoF) of the device, constituting a (hydrodynamic) coupling between these modes of motion.

The existence of these convolution terms represents a significant drawback both for motion simulation and for modern analysis/design of control/estimation strategies. From a motion simulation point of view, it is well known that the explicit computation of the convolution operator is computationally inefficient, often worsened by the necessity of a small (time) discretisation step to obtain accurate numerical integration. From a control/estimation theory point of view, the presence of these convolution mappings complicates the application of well-established results in the field, since modern control/estimation techniques are based on the availability of a state-space representation (at least in local coordinates) of the system under analysis (Faedo et al., 2017). Motivated by these drawbacks, researchers often seek for a parametric approximation of this radiation force subsystem in terms of a linear time-invariant dynamic representation, making explicit use of the corresponding hydrodynamic characteristics of the device obtained from BEM solvers.

To be precise, the prevailing approach is to approximate each convolution term independently (see, for example, (Giorgi and Ringwood, 2019, Pérez and Fossen, 2008)), as a single-input single-output (SISO) dynamic system, although the problem is inherently multiple-input multiple-output (MIMO), as a consequence of the multi-DoF characteristic of the WEC. One main disadvantage of this "multi-SISO" approach is that treating each convolution term independently often leads to an unnecessary high-order dimensional parameterisation of the radiation force subsystem, potentially rendering any control/estimation strategy challenging for real-time applications (Faedo et al., 2017).

We have recently presented a moment-matching-based MIMO identification method for wave energy applications in (Peña-Sanchez et al., 2019b), particularly to approximate the response of an array of WECs, i.e. a "farm" of multiple 1-DoF devices. This strategy is based on the underlying theoretical concepts developed in (Faedo et al., 2018b), and it allows for the computation of a model that exactly matches the frequency response of the target MIMO system at a set of user-selected frequencies $\mathscr{F}$, providing an efficient and accurate method to compute a state-space representation for the WEC dynamics. Additionally, a wise selection of the set $\mathscr{F}$ within this moment-based approach helps to enforce the underlying (physical) properties of the WEC under analysis.

Motivated by these results, in this paper we present an adaptation of the MIMO identification framework developed in (Peña-Sanchez et al., 2019b) to compute a parametric approximation of the radiation force subsystem of a multi-DoF device. We demonstrate that treating the approximation of radiation forces with our MIMO moment-based strategy (instead of the usual "multi-SISO" approach) provides a highly accurate low-dimensional system, hence offering a reliable parametric model

while also reducing the computational effort required for time-domain simulations and control/estimation calculations. Moreover, we show that we can guarantee physical properties of radiation forces in the approximating model, such as bounded-input bounded-output (BIBO) stability.

The remainder of this paper is organised as follows. The section titled "Moments for MIMO Systems" recalls the theory behind moment-matching for MIMO systems. The section titled "Equations of Motion for a Multi-DoF WEC" briefly discusses modelling of multi-DoF WECs in both the time and frequency domains. The section titled "Moment-Based Radiation System" presents a moment-domain analysis of radiation forces, while the section titled "Models Achieving Moment-Matching" discusses a moment-based algorithm to compute a parametric approximation for the radiation force subsystem of a multi-DoF WEC. The section "Application to a Corporate-like Device" discusses an application case, where a CorPower-like device (see Fig. 1a) is considered. Finally, "Conclusions" encompasses the main conclusions of this study.

Notation and Preliminaries

Standard notation is considered through this study, with any exceptions detailed in this section. $\mathbb{R}^+$ ($\mathbb{R}^-$) denotes the set of non-negative (non-positive) real numbers. $\mathbb{C}^0$ denotes the set of pure-imaginary complex numbers, and $\mathbb{C}_{<0}$ denotes the set of complex numbers with a negative real part. The symbol 0 stands for any zero element, dimensioned according to the context. The symbol $\mathbb{I}_n$ denotes an order n identity matrix. The spectrum of a matrix $A \in \mathbb{R}^{n\times n}$, i.e., the set of its eigenvalues, is denoted as $\lambda(A)$. The notation $W^\dagger$, with $W \in \mathbb{R}^{n\times m}$, denotes the Moore–Penrose inverse of W. The symbol $\bigoplus_{i=1}^{n}$ denotes the direct sum of n matrices, i.e., $\bigoplus_{i=1}^{n} A_i = \mathrm{diag}(A_1, A_2, \ldots, A_n)$. The expression $\|X\|_F$ denotes the Frobenius norm of the matrix X. The Kronecker product between two matrices $M_1 \in \mathbb{R}^{n\times m}$ and $M_2 \in \mathbb{R}^{p\times q}$ is denoted as $M_1 \otimes M_2 \in \mathbb{R}^{np\times mq}$. The convolution between two functions f and g over a set $\Omega \subset \mathbb{R}$, i.e., $\int_\Omega f(\tau)g(t-\tau)d\tau$ is denoted as $f * g$. The Fourier transform of a function $f \in L^2(\mathbb{R})$ is denoted by $\mathscr{F}\{f(t)\} = \hat{f}(j\omega)$, while its Laplace transform is denoted as $\mathscr{L}\{f(t)\} = F(s)$, where $L^2(\mathbb{R}) = \left\{f : \mathbb{R} \to \mathbb{C} | \int_{\mathbb{R}} |f(t)^2| dt < +\infty\right\}$. The notation $\Re\{z\}$ and $\Im\{z\}$ denote the real and imaginary parts of $z \in \mathbb{C}$. The symbol $e_{ij}^q \in \mathbb{R}^{q\times q}$ denotes a matrix with 1 in the ij component and 0 elsewhere. Finally, the symbol $\varepsilon_n \in \mathbb{R}^{n\times 1}$ denotes a vector with odd components equal to 1 and even components equal to 0.

MOMENTS FOR MIMO SYSTEMS

We note that the theory recalled herein is originated within the field of model order reduction in (Astolfi, 2010), being adapted for the WEC identification problem in (Faedo et al., 2018b, 2019, Peña-Sanchez et al., 2019b). The interested reader is referred to (Scarciotti and Astolfi, 2017, Chapter 1) for a thorough discussion on different model order reduction techniques and, particularly, on moment-based methods.

Consider a finite-dimensional, MIMO, continuous-time system Σ described, for $t \in \mathbb{R}^+$, by the state-space model

$$\Sigma : \begin{cases} \dot{x}(t) = Ax(t) + Bu(t), \quad y(t) = Cx(t), \end{cases} \tag{1}$$

with $x(t) \in \mathbb{R}^n$, $u(t) \in \mathbb{R}^q$, $y(t) \in \mathbb{R}^q$, $A \in \mathbb{R}^{n\times n}$, $B \in \mathbb{R}^{n\times q}$, and $C \in \mathbb{R}^{q\times n}$. Note that we focus on square systems, in line with the radiation force subsystem application. Consider the transfer function $W : \mathbb{C} \to \mathbb{C}^{q\times q}$, computed in terms of the associated impulse response matrix $w(t) = Ce^{At}B$ with $w_{ij} \in L^2(\mathbb{R})$, where w_{ij} denotes the ij element of w, as

$$\mathscr{L}\{w(t)\} \mapsto W(s) = C(s\mathbb{I}_n - A)^{-1}B, \tag{2}$$

and assume that (1) is minimal, i.e., controllable and observable.

Definition 1. (Astolfi, 2010) The 0 moment of system (1) at $s_i \in \mathbb{C}\backslash\lambda(A)$ is the complex matrix $\eta_0(s_i) = C(s_i\mathbb{I}_n - A)^{-1}B$. The k moment of system (1) at $s_i \in \mathbb{C}$ is the complex matrix

$$\eta_k(s_i) = \frac{(-1)^k}{k!}\left[\frac{d^k}{ds^k}W(s)\right]_{s=s_i}, \tag{3}$$

with $k \geq 1$ integer.

Remark 1. Note that moments, as in Definition 1, are the coefficients of the Laurent expansion of the transfer function $W(s)$ about the complex point s_i.

Remark 2. The idea of the moment-based model order reduction technique is based on interpolating the transfer function of the original system (and the derivatives of this) and the transfer function of the reduced order model (and the derivatives of this) at these interpolation points s_i.

The pioneering study (Astolfi, 2010) shows that the moments of a SISO linear system are in a one-to-one relation with the steady-state response (provided it exists) of the output of the interconnection between a signal generator and the system Σ itself. This concept is formally extended to MIMO systems in (Faedo et al., 2019, Peña-Sanchez et al., 2019b), and briefly recalled in the following theorem.

Theorem 1. (Faedo et al., 2019, Peña-Sanchez et al., 2019b) Consider system (1) and the autonomous multiple-output signal generator

$$\mathscr{G} : \begin{cases} \dot{\Xi}(t) = (\mathbb{I}_q \otimes S)\,\Xi(t), \quad u(t) = L\,\Xi(t), \end{cases} \tag{4}$$

with $\Xi(t) \in \mathbb{R}^{q\nu}$, $S \in \mathbb{R}^{\nu\times\nu}$, $L \in \mathbb{R}^{q\times q\nu}$, $\Xi(0) \in \mathbb{R}^{q\nu}$, $\lambda(A) \subset \mathbb{C}_{<0}$, $\lambda(S) \subset \mathbb{C}^0$, and the eigenvalues of S are simple. Suppose the triple of matrices $\left(L, \mathbb{I}_q \otimes S, \Xi(0)\right)$ is minimal. Let $\Pi \in \mathbb{R}^{n\times q\nu}$ be the (unique) solution of the Sylvester equation

$$A\Pi + BL = \Pi(\mathbb{I}_q \otimes S). \tag{5}$$

Then, there exists a one-to-one relation between the moments $\eta_0(s_1)$, $\eta_0(s_2)$, …, $\eta_0(s_\nu)$, with $s_i \in \lambda(S)$ for all $i \in \mathbb{N}_\nu$, and the steady-state response $C\Pi\Xi$ of the output y of the interconnection of system (1) with the signal generator (4).

Remark 3. The minimality of the triple $\left(L, \mathbb{I}_q \otimes S, \Xi(0)\right)$ implies the observability of the pair $\left(L, \mathbb{I}_q \otimes S\right)$ and the excitability of the pair $\left(\mathbb{I}_q \otimes S, \Xi(0)\right)$.

Remark 4. From now on, we refer to the matrix $C\Pi \equiv \underline{\mathcal{Y}}$, with Π the solution of (5), as the moment-domain equivalent of y.

Following this steady-state interpretation of moments, we now recall from (Astolfi, 2010) the formal definition of a reduced order model achieving moment-matching for system (1).

Definition 2. (Astolfi, 2010) Consider system (1) and the signal generator (4). The system described by the equations

$$\Sigma_{\mathscr{G}} : \begin{cases} \dot{\Theta}(t) = F\,\Theta(t) + G\,u(t), \quad \theta(t) = Q\,\Theta(t), \end{cases} \tag{6}$$

with $\Theta \in \mathbb{R}^{q\nu}$, $\theta(t) \in \mathbb{R}^q$, $F \in \mathbb{R}^{q\nu\times q\nu}$, $G \in \mathbb{R}^{q\nu\times q}$, and $Q \in \mathbb{R}^{q\times q\nu}$ is a model of system (1) at S if system (6) has the same moments at S as system (1).

Lemma 1. (Astolfi, 2010) Consider system (1) and the signal generator (4). Then, the system defined in (6) is a model of system (1) at S if $\lambda(F) \cap \lambda(S) = \emptyset$ and

$$\underline{\mathcal{Y}} = QP, \tag{7}$$

where $\underline{\mathcal{Y}} = C\Pi$ is the moment-domain equivalent of the output of system (1) computed from (5), and P is the unique solution of the Sylvester equation

$$FP + GL = P(\mathbb{I}_q \otimes S). \tag{8}$$

Remark 5. The transfer function of system $\Sigma_{\mathscr{G}}$ interpolates the transfer function of system Σ at the eigenvalues of the matrix S. Equivalently,

the steady-state output of the reduced order model (6) exactly matches the steady-state output of the system resulting from the interconnection of systems (1) and (4).

Given the characteristics of $\lambda(S)$ in Theorem 1, we set a standing assumption on the matrix S and we recall a useful lemma from (Faedo et al., 2019) that provides an alternative path for the computation of the matrix $\underline{\mathcal{Y}} = C\Pi$ in terms of the impulse response matrix of Σ.

Assumption 1. Consider the finite set $\mathscr{F} = 0 \cup \{\omega_p\}_{p=1}^{f} \subset \mathbb{R}^+$. The matrix S in (4) is written in block-diagonal form as

$$S = 0 \oplus \left(\bigoplus_{p=1}^{f} \begin{bmatrix} 0 & \omega_p \\ -\omega_p & 0 \end{bmatrix} \right), \tag{9}$$

where $\nu = 2f + 1$, $f \geq 0$ integer.

Lemma 2. (Faedo et al., 2019, Peña-Sanchez et al., 2019b) Consider the interconnection between system (1) and the signal generator (4), and suppose Assumption 1 holds. Without losing generality, assume that $\Xi(0) = [1 \ \varepsilon_{\nu-1}^{\intercal}]^{\intercal}$ so that the minimality of the triple $(L, \mathbb{I}_q \otimes S, \Xi(0))$ holds as long as the pair $(L, \mathbb{I}_q \otimes S)$ is observable. Then, the moment-domain equivalent $\underline{\mathcal{Y}}$ can be computed from the impulse response of Σ as

$$\underline{\mathcal{Y}} = \sum_{i=1}^{q} \sum_{j=1}^{q} e_{ij}^{q} L \left(\mathbb{I}_q \otimes \mathscr{R}_{ij}^{w} \right), \tag{10}$$

where each $\mathscr{R}_{ij}^{w} \in \mathbb{R}^{\nu \times \nu}$ is a block-diagonal matrix defined by

$$\mathscr{R}_{ij}^{w} = W_{ij}(0) \oplus \left(\bigoplus_{p=1}^{f} \begin{bmatrix} \Re\{W_{ij}(j\omega_p)\} & \Im\{W_{ij}(j\omega_p)\} \\ -\Im\{W_{ij}(j\omega_p)\} & \Re\{W_{ij}(j\omega_p)\} \end{bmatrix} \right), \tag{11}$$

and $W_{ij}(s) = \mathscr{L}\{w_{ij}(t)\}$.

Remark 6. Note that, following Lemma 2, each ω_p in (9) represents a desired interpolation point for the model reduction process, i.e., a frequency where the transfer function of system $\Sigma_{\mathscr{G}}$ matches the transfer function of the original system Σ.

Remark 7. The set $\mathscr{F}$, as defined in this study, inherently incorporates the zero element; i.e., we always consider matching at $s = 0$. This is particularly useful for a proper parameterisation of the radiation force subsystem, as it helps to enforce physical properties (see "Moment-Based Radiation Systems").

EQUATIONS OF MOTION FOR A MULTI-DoF WEC

We now introduce the key concepts behind linear modelling of multi-DoF WECs, both in the time and frequency domains. The assumptions considered herein are consistent across a wide variety of WEC control/estimation studies such as (Faedo et al., 2019).

Equations in the Time Domain

The motion for a WEC with N DoF can be expressed in the time domain according to Newton's second law, obtaining the following linear hydrodynamic formulation:

$$M\ddot{\chi}(t) = \mathcal{F}_r(t) + \mathcal{F}_h(t) + \mathcal{F}_e(t), \tag{12}$$

where $M = \bigoplus_{i=1}^{N} m_i$ is the mass matrix of the buoy with $m_i \in \mathbb{R}^+$ the mass of the ith DoF, and the elements of the vectors $\{\chi(t), \mathcal{F}_e(t), \mathcal{F}_h(t), \mathcal{F}_r(t)\} \subset \mathbb{R}^N$ contain the excursion x_i, excitation force f_{e_i}, hydrostatic restoring force f_{h_i}, and radiation force f_{r_i} acting on the ith DoF, with $i \in \mathbb{N}_N$, respectively.

The linearised hydrostatic force $\mathcal{F}_h$ can be written as $-S_h\chi$, where the matrix $S_h \in \mathbb{R}^{N \times N}$ is defined as $S_h = \sum_{i=1}^{N} \sum_{j=1}^{N} e_{ij}^{N} \otimes s_{h_{ij}}$ and contains the hydrostatic stiffness of each DoF (if $i = j$) and each interaction between the different modes of motion of the device due to the movement of each other DoF (if $i \neq j$). The radiation force $\mathcal{F}_r$ is modelled from linear potential theory and, using Cummins' equation (Cummins, 1962), is

$$\mathcal{F}_r(t) = -\mu_\infty \ddot{\chi}(t) - \int_{\mathbb{R}^+} K(\tau)\dot{\chi}(t-\tau)d\tau, \tag{13}$$

where $\mu_\infty = \lim_{\omega \to +\infty} A(\omega)$ represents the added-mass matrix at infinite frequency (Falnes, 2002) and $K(t) = \sum_{i=1}^{N} \sum_{j=1}^{N} e_{ij}^{N} \otimes k_{ij}(t) \in \mathbb{R}^{N \times N}$, $k_{ij} \in L^2(\mathbb{R})$ contains the (causal) radiation impulse response of each DoF (if $i = j$) and each interaction due to radiated waves created by the motion of other DoF (if $i \neq j$). Finally, we can express the linearised equation of motion of the multi-DoF WEC as

$$(M + \mu_\infty)\ddot{\chi}(t) + K(t) * \dot{\chi}(t) + S_h\chi(t) = \mathcal{F}_e(t). \tag{14}$$

Equations in the Frequency Domain

Applying the Fourier transform to (14) and considering the velocity of each DoF a measurable output (i.e., $\dot{\chi}(t)$), the following representation

$$\hat{\dot{\chi}}(j\omega) = \hat{\mathcal{F}}_e(j\omega)H(j\omega), \tag{15}$$

where $H : \mathbb{C}^0 \to \mathbb{C}^{N \times N}$ denotes the force-to-velocity frequency response mapping of the WEC, holds. The response $H(j\omega)$ can be readily computed (Falnes, 2002) as

$$H(j\omega) = \left(B(\omega) + j\omega \left(A(\omega) + M \right) + \frac{S_h}{j\omega} \right)^{-1}, \tag{16}$$

where $B(\omega)$ and $A(\omega)$ represent the radiation damping and the radiation added mass matrix of the device, respectively. These parameters are calculated using hydrodynamic codes at a finite set of uniformly spaced frequency samples $\Omega = \{\omega_i\}_{i=1}^{M}$ with $\Omega \subset [\omega_l, \omega_u]$, where ω_l and ω_u represent the lower and upper bounds of the range, respectively. We note that the ideal frequency range depends explicitly on the application, as discussed in (Faedo et al., 2018b).

Mapping Between Time and Frequency

Following the study performed in (Ogilvie, 1964), we recall that there exists a straightforward relation between the parameters of the models (14) and (15), which can be readily obtained via a direct application of the Fourier transform as

$$\begin{aligned} B(\omega) &= \int_{\mathbb{R}^+} K(t)\cos(\omega t)dt, \\ A(\omega) &= \mu_\infty - \frac{1}{\omega}\int_{\mathbb{R}^+} K(t)\sin(\omega t)dt. \end{aligned} \tag{17}$$

Then, the radiation force impulse response mapping $K : \mathbb{R}^+ \longrightarrow \mathbb{R}^{N \times N}$ can be directly written (Falnes, 2002) as

$$K(t) = \frac{2}{\pi}\int_{\mathbb{R}^+} B(\omega)\cos(\omega t)d\omega. \tag{18}$$

Considering Equation (18), the frequency-domain representation of the radiation force kernel K can be obtained as

$$K(j\omega) = B(\omega) + j\omega\left[A(\omega) - \mu_\infty\right]. \tag{19}$$

Property	**Significance on K**
(I) $\lim_{\omega \to +\infty} K(j\omega) = 0$	Strictly proper
(II) $\lim_{t \to +\infty} K(t) = 0$	BIBO stable
(III) $\lim_{\omega \to 0} K(j\omega) = 0$	With transmission zeros at the origin
(IV) $\Re\{K_{ii}(j\omega)\} > 0, \ \forall i \in \mathbb{N}_N$	Passivity (see Khalil (1996) for a proof).

Table 1 Properties of the radiation kernel K

The radiation kernel frequency response $K(j\omega)$ has a set of particular properties that have been used in the literature to enforce a structure on the parametric model used to identify the frequency-domain data. Such properties are recalled in Table 1.

MOMENT-BASED RADIATION SYSTEM

The radiation impulse response mapping defines a linear-time invariant system completely characterised by $K : \mathbb{R}^+ \longrightarrow \mathbb{R}^{N\times N}$, where its input is the vector containing the device velocities for each DoF, i.e., $\dot{\chi}$. To be precise, the radiation subsystem Σ^K is given by

$$\Sigma_K : \theta_K(t) = K(t) * \dot{\chi}(t), \tag{20}$$

where $\theta_K(t) \in \mathbb{R}^N$ is the output (radiation force) of system Σ_K.

With the definition of Σ_K, and following the theory presented in "Moments for MIMO Systems," we can obtain a parametric model $\tilde{\Sigma}_{K\mathscr{F}}$ for the radiation force subsystem defined in (20) using the result of Lemma 2, which offers an explicit computation of the moment-domain equivalent of a system in terms of its impulse response mapping. To that end, and in the spirit of Assumption 1, we express the velocity of the multi-DoF WEC $\dot{\chi}$ as an autonomous multiple-output signal generator in a similar fashion to $\mathscr{G}$ in (4), i.e.,

$$\mathscr{G}_{\dot{\chi}} : \begin{cases} \dot{\Xi}_{\dot{\chi}}(t) = (\mathbb{I}_N \otimes S)\, \Xi_{\dot{\chi}}(t), \quad \dot{\chi}(t) = L_{\dot{\chi}}\, \Xi_{\dot{\chi}}(t), \end{cases} \tag{21}$$

with S as in (9), $\dot{\Xi}_{\dot{\chi}}(0) = [1\ \epsilon_{\nu-1}^{\intercal}]^{\intercal}$ and $L_{\dot{\chi}}$ such that the pair $(L_{\dot{\chi}}, S)$ is observable. Then, recalling the result of Lemma 2, the moment-domain equivalent of the output of system Σ_K in (20) can be straightforwardly computed as

$$\underline{\mathcal{Y}}_K = \sum_{i=1}^{N}\sum_{j=1}^{N} e_{ij}^N L_{\dot{\chi}} \left(\mathbb{I}_N \otimes \mathscr{R}_{ij}^k\right), \tag{22}$$

where each $\mathscr{R}_{ij}^k \in \mathbb{R}^{\nu\times\nu}$ is a block-diagonal matrix defined by

$$\mathscr{R}_{ij}^k = 0 \oplus \left(\bigoplus_{p=1}^{f} \begin{bmatrix} \Re\{K_{ij}(j\omega_p)\} & \Im\{K_{ij}(j\omega_p)\} \\ -\Im\{K_{ij}(j\omega_p)\} & \Re\{K_{ij}(j\omega_p)\} \end{bmatrix} \right). \tag{23}$$

Note that each entry of $\mathscr{R}_{ij}^k$ directly depends on the hydrodynamic coefficients computed with BEM solvers. To be precise, let $A_{ij}(\omega)$ and $B_{ij}(\omega)$ be the ijth element of the added mass matrix $A(\omega)$ and the radiation damping matrix $B(\omega)$ of the device, respectively. Then,

$$\begin{aligned} \Re\{K_{ij}(j\omega_p)\} &= B_{ij}(\omega_p), \\ \Im\{K_{ij}(j\omega_p)\} &= \omega_p \left[A_{ij}(\omega_p) - \mu_{\infty_{ij}}\right], \end{aligned} \tag{24}$$

where $\mu_{\infty ij}$ is the ij-th element of the matrix μ_∞.

Remark 8. Note that each matrix $\mathscr{R}_{ij}^k$ already incorporates the hydrodynamic property $K_{ij}(0) = 0$ (see Table 1, Property III).

Finally, following Definition 2 and Lemma 1, we note that the parametric (state-space) description

$$\tilde{\Sigma}_{K\mathscr{F}} : \begin{cases} \dot{\Theta}_K(t) = F_K\Theta_K(t) + G_K\chi(t)\ \tilde{\theta}_K(t) = Q_K\Theta_K(t), \end{cases} \tag{25}$$

is a system that interpolates the target frequency response $K(j\omega)$ at the set $\mathscr{F}$; i.e., it has the exact same frequency response of the radiation subsystem Σ_K at the frequencies defined in the set $\mathscr{F}$, if $Q_K P_K = \underline{\mathcal{Y}}_K$, where $P_K \in \mathbb{R}^{\nu\times\nu}$ is the unique solution of the Sylvester equation

$$F_K P_K + G_K L_{\dot{\chi}} = P_K(\mathbb{I}_N \otimes S), \tag{26}$$

and $\underline{\mathcal{Y}}_K$ is computed from Equation (22). The explicit computation of the matrices F_K, G_K, Q_K in (25) (fulfilling condition (26)) is addressed in the following section.

MODELS ACHIEVING MOMENT-MATCHING

Herein, we briefly summarise some of the key concepts behind the algorithm proposed in (Peña-Sanchez et al., 2019b) to compute a moment-based time-domain model for an array of WECs, and we adapt the procedure for our multi-DoF radiation force subsystem case. We note that (Peña-Sanchez et al., 2019b) regard the moment-based concepts described in this study in synergy with well-known results of subspace-based identification methods, as detailed in (McKelvey et al., 1996).

To be precise, we approximate the dynamic and output matrix from the target radiation subsystem Σ_K in terms of the corresponding singular value decomposition of the Hankel matrix $\mathscr{H}$ (see (McKelvey et al., 1996)), constructed from $K(j\omega)$ as defined in (19) and computed at the finite set of uniformly spaced frequencies Ω (see "Equations of Motion for a Mult-DoF WEC"). These α-dimensional approximated matrices ${}^d\hat{A}_\alpha \in \mathbb{R}^{\alpha\times\alpha}$, $\hat{C}_\alpha \in \mathbb{R}^{N\times\alpha}$ (where ${}^d\hat{A}_\alpha$ corresponds to a discrete-time model) can be computed as

$${}^d\hat{A}_\alpha = (J_1\hat{U}_\alpha)^\dagger J_2 \hat{U}_\alpha, \quad \hat{C}_\alpha = J_3\hat{U}_\alpha \tag{27}$$

where the continuous-time equivalent matrix $\hat{A}_\alpha$ can be obtained directly from ${}^d\hat{A}_\alpha$ using, for instance, the bilinear transformation. We refer the reader to (McKelvey et al., 1996) for the explicit expression of the matrices J_1, J_2, J_3, and $\hat{U}_\alpha$.

Remark 9. If ${}^d\hat{A}_\alpha$, computed as in (27), has unstable eigenvalues, one can always project such a set into the complex unit circle following the procedure described in (McKelvey et al., 1996).

Finally, the moment-based identification algorithm for the radiation force subsystem utilised herein can be summarised in the following steps:

I Select a set of f interpolation points (frequencies ω_p) $\mathscr{F} = 0 \cup \{\omega_p\}_{p=1}^f$ to achieve moment-matching.

II Compute the matrix $\mathbb{I}_N \otimes S$ following (9) and select any $L_{\dot{\chi}}$ such that the pair $(L_{\dot{\chi}}, \mathbb{I}_N \otimes S)$ is observable.

III Calculate the moment-domain equivalent of the output of system (20) $\underline{\mathcal{Y}}_K$ using Equation (22).

IV Compute the matrices $\hat{A}_{N\nu}$ and $\hat{C}_{N\nu}$ from (27).

V Consider the parametric model for the radiation subsystem described in (25) and set $F_K = \hat{A}_{N\nu}$ and $Q_K = \hat{C}_{N\nu}$.

VI Consider the frequency response of (25), i.e.,

$$\tilde{K}(j\omega, G_K) = Q_K\,(j\omega_i - F_K)^{-1}\, G_K.$$

Using the frequency set $\Omega = \{\omega_i\}_{i=1}^M$, compute the input matrix G_K^{opt} with the following optimisation-based procedure:

$$G_K^{\text{opt}} = \arg\min_{G_K} \sum_{i=1}^{M} \left\| \tilde{K}(j\omega_i, G_K) - K(j\omega_i) \right\|_F^2$$

subject to

$$F_K P_K + G_K L_{\dot{\chi}} = P_K(\mathbb{I}_N \otimes S), \quad Q_K P_K = \underline{\mathcal{Y}}_K.$$

VII Compute a $N\nu$-dimensional radiation force subsystem time-domain model $\tilde{\Sigma}_{K\mathscr{F}}$ achieving moment-matching at S as

$$\tilde{\Sigma}_{K\mathscr{F}} : \begin{cases} \dot{\Theta}_K(t) = F_K\,\Theta_K(t) + G_K^{\text{opt}}\dot{\chi}(t), \quad \tilde{\theta}_K(t) = Q_K\,\Theta_K(t). \end{cases}$$

Remark 10. The method is based on the idea of building the model $\tilde{\Sigma}_{K\mathscr{F}}$ by matching the $f + 1$ (user-defined) frequencies of the set $\mathscr{F}$, exploiting the system structure of (25), and solving for an equality-constrained optimisation problem, which computes the input matrix G_K^{opt} that minimises the difference between the target frequency response and that of (25), while ensuring the moment-matching conditions in the model.

APPLICATION TO A CORPOWER-LIKE DEVICE

To illustrate the strategy proposed in this study, we consider the CorPower-like device utilised in (Giorgi and Ringwood, 2019) (note that the applicability of the method is independent of the specific device geometry) and depicted here in Figure 1a. We refer the reader to (Giorgi and Ringwood, 2019) for a precise description of the dimensions of this device.

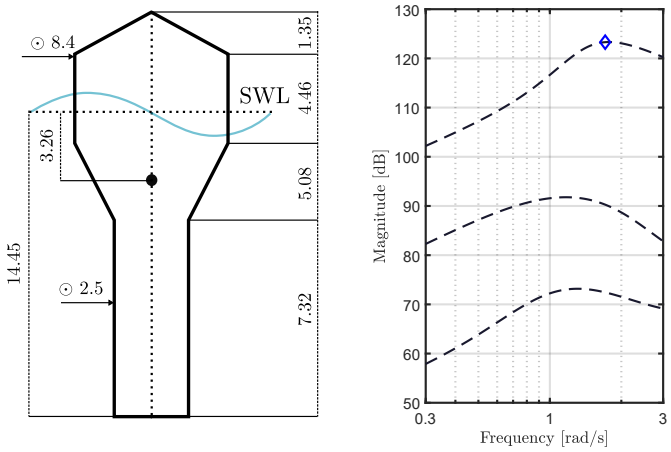

(a) Schematic of the device (b) Singular values plot for $K(j\omega)$

Fig. 1 CorPower-like device considered in this study; SWL, still water level

Following the analysis carried out in (Giorgi and Ringwood, 2019), we consider surge (mode 1), heave (mode 2), and pitch (mode 3) as the more relevant DoF for this particular application case. The corresponding hydrodynamic parameters $A(\omega)$ and $B(\omega)$ can be appreciated in Fig. 2. Note that the elements $\{1,2\},\{2,1\},\{2,3\},\{3,2\}$ of the matrices $A(\omega)$ and $B(\omega)$ are not shown in Fig. 2, given that there is no interaction due to radiation forces between these particular modes of motions; i.e., they are exactly zero for all $\omega \in \mathbb{R}^+$. The maximum frequency selected in the BEM code, to compute the hydrodynamic parameters of the CorPower-like device of Fig. 2, is set to 10 [rad/s]. Nevertheless, we note that ocean waves peak periods typically lie between 3 [s] and 16 [s], which implies that the frequency range of the wave excitation force $\mathcal{F}_e$ is approximately [0.4, 2.1] [rad/s] (Faedo et al., 2018b). Hence, it is straightforward to conclude that, under the modelling assumptions considered in "Equations of Motion for a Multi-DoF WEC," the velocity of the multi-DoF device (input to Σ_K) has significant frequency components in the same range.

From now on, we denote the frequency-domain model of the radiation subsystem corresponding to our CorPower-like device $K(j\omega)$ as the target response. In addition, we use the notation $K_{ij}(j\omega)$ for the ij element of the matrix $K(j\omega)$. More precisely, $K_{ij} : \mathbb{C}^0 \longrightarrow \mathbb{C}$ is the frequency response mapping between the output i (radiation force exerted on the ith mode) and the input j (velocity of the jth mode).

Approximation of the Radiation Subsystem

We now specifically proceed with the computation of a moment-based approximation $\tilde{\Sigma}_{K\mathscr{F}}$ for the radiation subsystem Σ_K, based on the knowledge of the target frequency response $K(j\omega)$ and using the procedure described in "Models Achieving Moment-Matching."

Recall that the first step of the algorithm is to select the set of frequencies $\mathscr{F}$ to interpolate. In the SISO case (1-DoF device) of (Faedo et al., 2018b), a sensible choice can be made by analysing the gain of $K(j\omega)$, and selecting dynamically important points, such as the resonant frequency of the particular DoF under study, i.e., where the maximum amplification occurs. For this MIMO case, it is well-known that the system gain depends on the corresponding input direction (see, for example, (Zhou and Doyle, 1998)), so that this set of dynamically important points cannot be obtained by inspecting each element $K_{ij}(j\omega)$ independently. Instead, we use the singular values of $K(j\omega)$ (Zhou and Doyle, 1998), which are plotted in Fig. 1b.

Following well-known theory for MIMO systems, it is straightforward to notice, from Fig. 1b, that $\omega \approx 1.7$ [rad/s] represents an interpolation point of dynamical importance (marked with a blue diamond in Fig. 1b), being the frequency where the maximum amplification occurs, i.e., the frequency characterising the $\mathscr{H}_\infty$-norm of the system (Zhou and Doyle, 1998).

Based on this, we propose two different frequency interpolation sets $\mathscr{F}$, as follows:

$$\mathscr{F}_1 = \{0, 1.7\}, \quad \mathscr{F}_2 = \{0, 0.8, 1.7\},$$

where $\mathscr{F}_2$ includes the set $\mathscr{F}_1$ and incorporates an additional low frequency component $\omega = 0.8$ [rad/s]. Note that both sets include the zero element (see Remark 7). Following the discussion provided at the beginning of this section, the frequency range selected to approximate $K(j\omega)$ is given by $\Omega = [0.3, 3]$ [rad/s], with a frequency discretisation step of 0.01 [rad/s]. Given that heave (mode 2) is the main DoF of this WEC, Fig. 3 presents the Bode diagram for the target response $K_{22}(j\omega)$ (dashed black) and the moment-based approximated response $\tilde{K}_{22}(j\omega)$ (solid gray) for both parametric models $\tilde{\Sigma}_{K\mathscr{F}_1}$ (left) and $\tilde{\Sigma}_{K\mathscr{F}_2}$ (right). The interpolation points for each model are denoted by an empty red circle. As expected, the approximated systems have the exact same frequency response as the target model for each corresponding set $\mathscr{F}$. Though using the set $\mathscr{F}_1$ as the interpolation set provides quite accurate results, the decrease in the approximation error from system $\tilde{\Sigma}_{K\mathscr{F}_1}$ to $\tilde{\Sigma}_{K\mathscr{F}_2}$ can be clearly appreciated.

As a conclusive graphical illustration of the frequency-domain performance for the models computed via our strategy, Fig. 4 presents the singular value plot for the target response $K(j\omega)$, and the approximated mapping $\tilde{K}(j\omega)$, both for $\tilde{\Sigma}_{K\mathscr{F}_1}$ (left) and $\tilde{\Sigma}_{K\mathscr{F}_2}$ (right). It can be readily appreciated that both models can accurately approximate the target singular values in every principal direction (i.e., the target MIMO gain) with an increase in accuracy when using the interpolation set $\mathscr{F}_2$ instead of $\mathscr{F}_1$.

Aiming to further assess the strategy, Table 2 offers a numerical appraisal of each of the moment-matching-based parametric models in terms of the following parameters:

Dim: Dimension (order) of the parametric model

NRMSE$_\mathbf{F}$: Normalized Root -Mean-Square Error (NRMSE) computed against the target WEC frequency response $\forall\ \omega \in \Omega$.

NRMSE$_\mathbf{T}$: NRMSE computed (in steady-state) against the target steady-state radiation system response using inputs generated with frequency content inside the set Ω. In order to get meaningful results for the time-domain scenario of Table 2, and since the inputs are generated from sets of random amplitudes, it is found that the mean of 10 simulations is necessary to obtain a 95% confidence interval with a half-width of 0.25% of the mean, computed as in (Peña-Sanchez et al., 2018).

The first row of Table 2 includes the "multi-SISO," which corresponds to a parametric model of the MIMO system Σ_K obtained by approximating each individual element of the matrix $K(j\omega)$ with a SISO system. Though several strategies can be used to obtain this "multi-SISO" system, we select herein the SISO moment-matching method described in (Faedo et al., 2018b) (with $\mathscr{F}_2$ as interpolation points), resulting in a model of dimension 25. This is merely motivated by the comparison

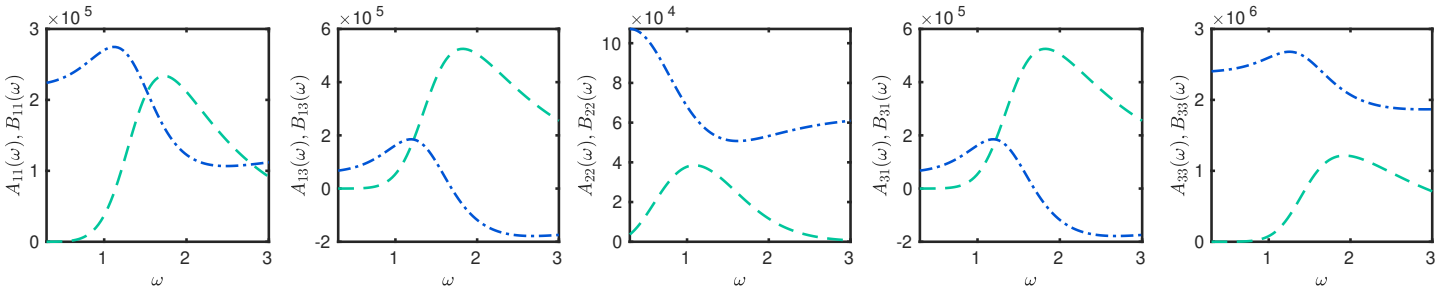

Fig. 2 Hydrodynamic parameters $A(\omega)$ (dot-dashed blue) and $B(\omega)$ (dashed green) for the CorPower-like device considered herein

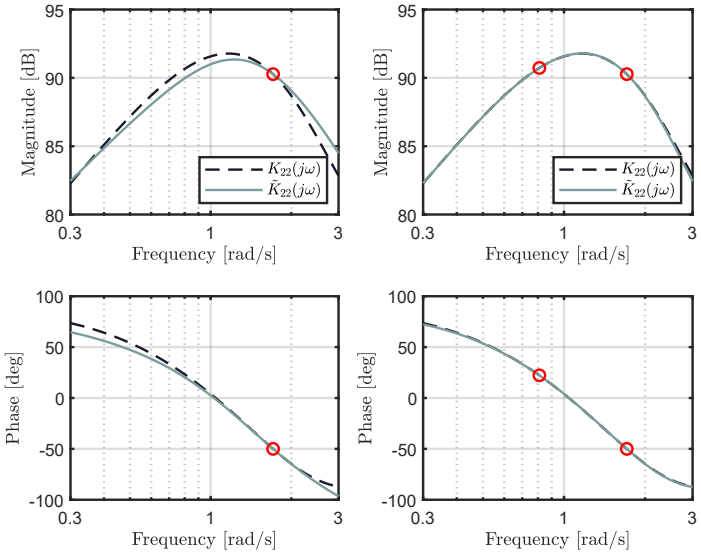

Fig. 3 Bode diagram for $K_{22}(j\omega)$ (dashed black), and $\tilde{K}_{22}(j\omega)$ (solid gray) for both parametric models $\tilde{\Sigma}_{K\mathscr{F}_1}$ (left) and $\tilde{\Sigma}_{K\mathscr{F}_2}$ (right), with interpolation points (empty red circles)

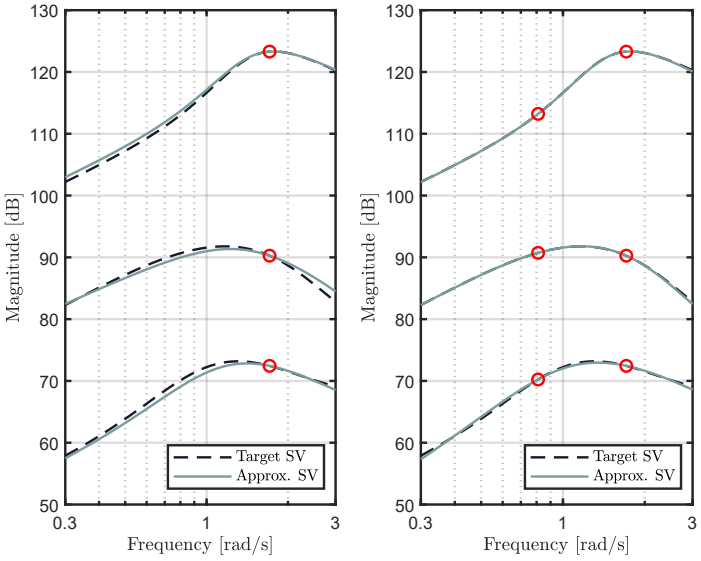

Fig. 4 Singular value (SV) plot for $K(j\omega)$ (dashed black) and $\tilde{K}(j\omega)$ (solid gray), with interpolation points (empty red circles)

study (Peña-Sanchez et al., 2019a), where the SISO moment-matching method is shown to outperform well-established strategies, both in terms of performance and preservation of physical characteristics.

Model	Dim	NRMSE_F	NRMSE_T
"multi-SISO"	28	1.036%	0.985%
$\tilde{\Sigma}_{\mathscr{F}_1}$	9	3.580%	4.045%
$\tilde{\Sigma}_{\mathscr{F}_2}$	15	1.092%	0.664%

Table 2 Numerical comparison table

As can be appreciated in Table 2, note that the approach proposed herein provides highly accurate results even with a single interpolation point (in addition to the zero frequency), with only approximately 4% of error in both the frequency domain and time domain, and with an intrinsic decrease in computational complexity, given the low dimension (order) of the resulting model. We also note that the "multi-SISO" approach provides similar results to those of $\tilde{\Sigma}_{K\mathscr{F}_2}$ with higher computational requirements (i.e., higher system order). That said, we emphasize that the radiation subsystem should be treated as a MIMO system when it comes to its parametric approximation.

To conclude the assessment of our strategy, we analyse the moment-based computed models $\tilde{\Sigma}_{K\mathscr{F}}$ with respect to the physical properties of the radiation subsystem listed in Table 1.

- *Property I (Σ_K is strictly proper)*: This property is always fulfilled by the family of parametric models defined in (25). See, for example, (Khalil, 1996).
- *Property II (Σ_K is BIBO stable)*: The strategy proposed in "Models Achieving Moment-Matching" preserves the dynamic matrix approximated by using the Hankel matrix associated with $K(j\omega)$. This matrix can always be constructed so that is Hurwitz (see Remark 10), and, hence, system $\tilde{\Sigma}_{K\mathscr{F}}$ is BIBO stable. By way of example, Fig. 5 shows the pole-zero map for system $\tilde{\Sigma}_{K\mathscr{F}_1}$ computed in this same section for the CorPower-like device. It can be appreciated that all the poles are contained in the open left-half of the complex plane; i.e., $\tilde{\Sigma}_{K\mathscr{F}_1}$ is BIBO stable.
- *Property III (Σ_K has transmission zeros at $s = 0$)*: This property is specifically enforced by considering 0 as part of the set of interpolation points $\mathscr{F}$ (see Remark 8). In practice, this can be (graphically) appreciated in the pole-zero map of Fig. 5, where the zero at $s = 0$ manifests explicitly for the approximating model $\tilde{\Sigma}_{K\mathscr{F}_1}$.
- *Property IV (Σ_K is passive)*: This particular physical property is not enforced by our strategy. However, we note that, if the target data $K(j\omega)$ effectively come from a passive model, the parametric models computed with our strategy, for the WEC radiation force subsystem, are virtually inherently passive. If required by the application, a similar strategy to that of (Faedo et al., 2018a) can be considered to specif-

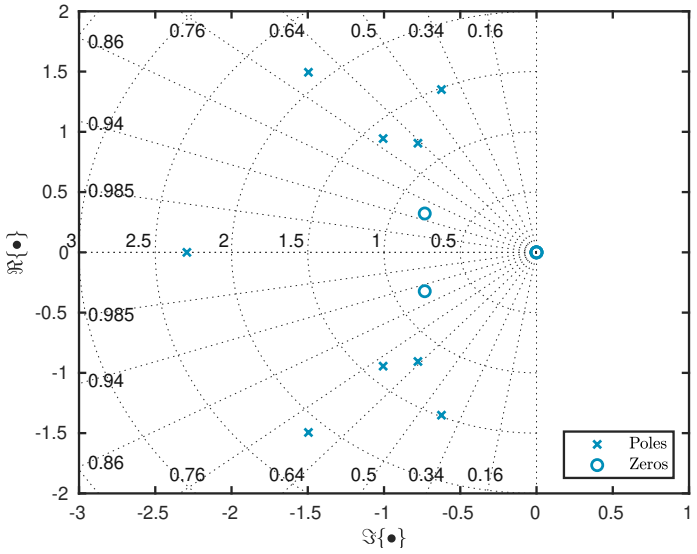

Fig. 5 Pole-zero map for the approximating model $\tilde{\Sigma}_{K\mathscr{F}_1}$

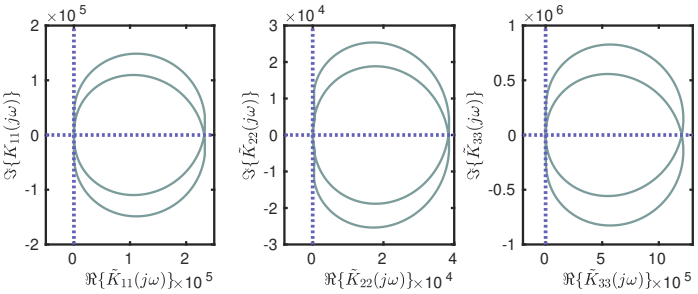

Fig. 6 Nyquist plot (diagonal elements) of $\tilde{K}(j\omega)$ for $\tilde{\Sigma}_{K\mathscr{F}_2}$

ically ensure passivity within this multi-DoF moment-based framework. Figure 6 depicts the Nyquist plot for the diagonal elements of $\tilde{K}(j\omega)$ for $\tilde{\Sigma}_{K\mathscr{F}_2}$, where it can be appreciated that $\Re\{\tilde{K}_{ii}(j\omega)\} > 0$ for all $i \in \mathbb{N}_3$ and, hence, $\Sigma_{K\mathscr{F}_2}$ is passive.

CONCLUSIONS

This paper presents a MIMO moment-based identification framework for the radiation force subsystem of multi-DoF WECs. The proposed strategy computes a parametric model of the target radiation force mapping using raw frequency-domain data produced by well-known BEM-based hydrodynamic codes. Such a moment-based model exactly matches the target steady-state response for a user-defined set of frequencies, allowing for the preservation of the relevant dynamic characteristics of the device. Moreover, we show that this parametric approximation retains important properties of radiation forces, such as input-output stability and passivity, agreeing with the underlying physics that characterise such a system. The performance of the strategy is demonstrated and analysed from both a time- and a frequency-domain perspective, using a CorPower-like multi-DoF device as application case.

ACKNOWLEDGMENT

The authors thank Prof. Alessandro Astolfi and Dr. Giordano Scarciotti from Imperial College London, for useful discussions on moments. This material is based upon works supported by Science Foundation Ireland under Grant no. 13/IA/1886.

REFERENCES

Astolfi, A. (2010). Model reduction by moment matching for linear and nonlinear systems. *IEEE Transactions on Automatic Control*, 55(10), 2321–2336.

Cummins, W. E. (1962). The impulse response function and ship motions. *Schiffstechnik*, 47, 101–109.

Faedo, N., Olaya, S., and Ringwood, J. V. (2017). Optimal control, MPC and MPC-like algorithms for wave energy systems: An overview. *IFAC Journal of Systems and Control*, 1, 37–56.

Faedo, N., Peña Sanchez, Y., and Ringwood, J. V. (2018a). Passivity preserving moment-based finite-order hydrodynamic model identification for wave energy applications. In *Advances in Renewable Energies Offshore, RENEW 2018*, 351–359.

Faedo, N., Peña-Sanchez, Y., and Ringwood, J. V. (2018b). Finite-order hydrodynamic model determination for wave energy applications using moment-matching. *Ocean Engineering*, 163, 251 – 263.

Faedo, N., Scarciotti, G., Astolfi, A., and Ringwood, J. V. (2019). Moment-based constrained optimal control of an array of wave energy converters. In *American Control Conference (ACC), Philadelphia*, 4797–4802.

Falnes, J. (2002). *Ocean waves and oscillating systems: linear interactions including wave-energy extraction*. Cambridge University Press.

Giorgi, G. and Ringwood, J. V. (2019). A compact 6-DoF nonlinear wave energy device model for power assessment and control investigations. *IEEE Transactions on Sustainable Energy*, 10(1), 119–126.

Khalil, H. K. (1996). *Nonlinear Systems*. Prentice-Hall, New Jersey.

Li, Y. and Yu, Y.-H. (2012). A synthesis of numerical methods for modeling wave energy converter-point absorbers. *Renewable and Sustainable Energy Reviews*, 16(6), 4352–4364.

McKelvey, T., Akçay, H., and Ljung, L. (1996). Subspace-based multivariable system identification from frequency response data. *IEEE Transactions on Automatic Control*, 41(7), 960–979.

Ogilvie, T. F. (1964). Recent progress toward the understanding and prediction of ship motions. In *5th Symposium on naval hydrodynamics*, 2–5. Bergen, Norway.

Peña-Sanchez, Y., Faedo, N., and Ringwood, J. V. (2019a). A critical comparison between parametric approximation methods for radiation forces in wave energy systems. In *Proceedings of the 29th International Offshore and Polar Engineering Conference (ISOPE), Honolulu, Hawaii*, 174–181.

Peña-Sanchez, Y., Faedo, N., and Ringwood, J. V. (2019b). Moment-based parametric identification of arrays of wave energy converters. In *American Control Conference (ACC), Philadelphia*, 4785–4790.

Peña-Sanchez, Y., Garcia-Abril, M., Paparella, F., and Ringwood, J. V. (2018). Estimation and forecasting of excitation force for arrays of wave energy devices. *IEEE Transactions on Sustainable Energy*, 9(4), 1672–1680.

Penalba, M., Kelly, T., and Ringwood, J. V. (2017). Using NEMOH for modelling wave energy converters: A comparative study with WAMIT. In *Proceedings of the 12th European Wave and Tidal Energy Conference, Cork*, 631.

Pérez, T. and Fossen, T. (2008). Joint identification of infinite-frequency added mass and fluid-memory models of marine structures. *Modeling, Identification and Control*, 29(3), 93–102.

Scarciotti, G. and Astolfi, A. (2017). Nonlinear model reduction by moment matching. *Foundations and Trends in Systems and Control*, 4(3-4), 224–409.

Zhou, K. and Doyle, J. C. (1998). *Essentials of robust control*, volume 104. Prentice hall Upper Saddle River, NJ.

View publication stats